

# Structure and Phase Composition of Alloyed Intermetallic Compound Ni<sub>3</sub>Al after Annealing and High-Temperature Creep

T. N. Vershinina<sup>a</sup>, O. A. Golosova<sup>a</sup>, Yu. R. Kolobov<sup>a</sup>, and K. B. Povarova<sup>b</sup>

<sup>a</sup>Scientific and Educational Center Nanostructured Materials and Nanotechnologies, Belgorod State University, Belgorod, Russia

e-mail: Vershinina@bsu.edu.ru

<sup>b</sup>Baikov Institute of Metallurgy and Materials Science, Russian Academy of Sciences, Leninskii pr. 49, Moscow, 119991 Russia

**Abstract**—The structure and phase composition of a VKNA-25 alloy based on the Ni<sub>3</sub>Al intermetallic compound, produced by directional solidification, and alloyed with rare-earth metals are studied in the following two states: after annealing at 1100°C and after creep at 1100°C.

## INTRODUCTION

Presently, the most important parts of gas-turbine aircraft engines and power plants, such as nozzle and rotating blades, operating under combined action of temperature and load are produced of nickel-based heat-resistant alloys (ZhS6U, MAR M-200, etc.). The application of alloys of this type is related to their high level of heat resistance, thermal stability of the structure, and reliable operation at temperatures up to 1050°C [1]. The service properties of these alloys are mainly improved by increasing the total concentration of high-melting-point elements (rhenium, tungsten, molybdenum, etc.). However, this well-known approach to the considered problem inevitably results in a high cost and specific weight of the alloys. Meanwhile, an increase in the weight of, e.g., an aircraft engine unavoidably results in a low thrust-to-weight ratio, an increased load applied to a rotor, and (hence) a decrease in the operation lifetime.

The necessity to increase operation temperatures of the parts of gas turbine engines led to the development of a novel class of high-temperature materials based on the Ni<sub>3</sub>Al intermetallic compound [1, 2]. The alloys based on the Ni<sub>3</sub>Al intermetallic compound are comparable with nickel heat-resistant alloys in terms of manufacturability and are characterized by numerous supplemental advantages, such as the melting point, the specific weight, and high oxidation resistance, which is related to the peculiar features of atomic bond in the intermetallic compound lattice and to the chemical composition of a surface protective oxide film [1, 3]. An increase in the thermal stability of the structure of such alloys can be achieved by alloying with rare-earth metals (REMs), which are not

dissolved in the solid solutions based on  $\gamma'$ -Ni<sub>3</sub>Al and  $\gamma$ -Ni and form nanosized phases that stabilize a dendritic or a directionally solidified single-crystal structure of cast alloys [1–8].

The life and reliability items made of heat-resistant alloys at high temperatures are mainly determined by their structural and phase stability, which depends in particular on the ratio of the volumetric portions and the morphology of phases. Therefore, we study the influence of thermal treatment and a simultaneous impact of temperature and load (during creep) on the structural-phase state of an Ni<sub>3</sub>Al-based alloy with REMs.

## EXPERIMENTAL

We studied a VKNA-25 nickel alloy based on Ni<sub>3</sub>Al, produced by directional solidification, and having the following basic composition (%):<sup>1</sup>

Al	Ti	Cr	Mo	W	Fe	Re	Co
8.4	0.5	4.97	5.0	3.11	0.1	1.5	3.95

The structural-phase state of a cast alloy with 0.3% La and a rodlike dendritic structure was studied after annealing at 1100°C for 563 h and upon creep tests at 95 MPa at the same temperature in 563 h.

We used scanning electron microscopy (SEM) in the backscattered electron mode, electron-probe microanalysis with a Quanta 600 FEG scanning electron microscope, transmission electron microscopy

<sup>1</sup> The element contents are given in wt % unless otherwise specified.

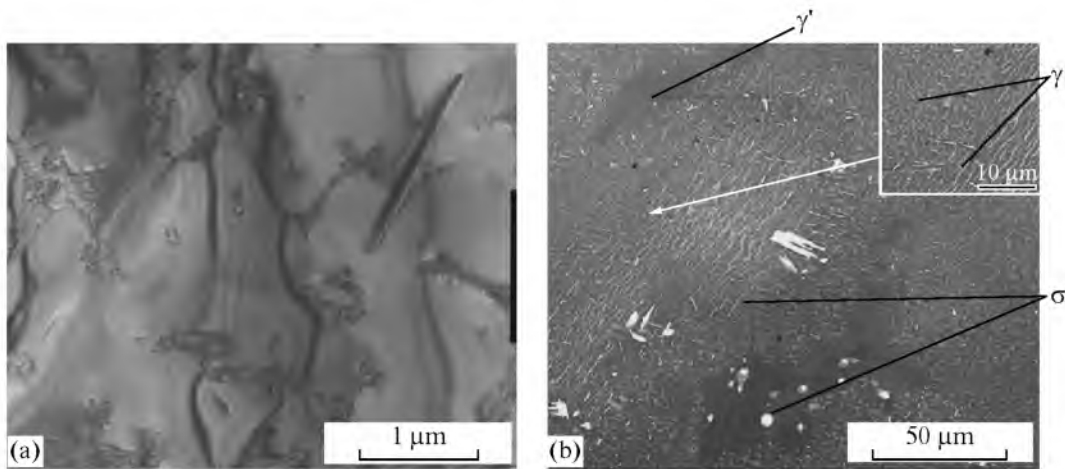


Fig. 1. Microstructure of the VKNA-25 alloy after annealing at 1100°C, 563 h: (a) TEM and (b) SEM.

(TEM) with a JEOL JEM2100 microscope at magnifications of 100–200 000, and X-ray diffraction with an ARL X'TRA X-ray diffractometer and  $\text{CuK}\beta$  radiation.

Preliminary preparation of a specimen surface for SEM analysis consisted of mechanical polishing with subsequent chemical etching in a 10% solution of nitric acid or electrolytic polishing with additional etching in a solution of 22% perchloric acid and 78% acetic acid (reagent grade).

Foils for TEM analysis were prepared using electrolytic polishing in a solution of 78% glacial acetic acid and 22% perchloric acid at 0°C. The final stage of thinning was performed with a Fishione ionic etching instrument to remove an oxide film after electrolytic polishing. Etching was performed simultaneously by two ionic argon beams when a specimen rotated at an inclination angle of 7° to an ion beam at an accelerating voltage of 3 kV and a beam current of 4 mA.

## RESULTS AND DISCUSSION

The main structural component of the alloy in all studied states is  $\gamma'$ -phase (alloyed intermetallic compound  $\text{Ni}_3\text{Al}$ ), its volume fraction is ~90%. This  $\gamma'$ -phase is separated by thin discontinuous layers of a disordered  $\gamma$ -matrix (nickel-based solid solution; Fig. 1a).

In accordance with the classification proposed in [5], the alloys of the considered type can contain four structural forms of the  $\gamma'$  phase of different sizes (scales). In order of decreasing size, they are denoted as  $\gamma'_I$ ,  $\gamma'_{II}$ ,  $\gamma'_{III}$ , and  $\gamma'_{IV}$ . The largest  $\gamma'$ -phase particles are referred to the first scale level ( $\gamma'_I$ ), and the particles of a fine  $\gamma + \gamma'$  mixture, to the second scale level ( $\gamma'_{II}$ ). The particles of the third ( $\gamma'_{III}$ ) and the fourth

( $\gamma'_{IV}$ ) scale levels precipitate in the course of aging and creep according to the reactions  $\gamma'_I \rightarrow \gamma + \gamma'_{III}$  and  $\gamma \rightarrow \gamma + \gamma'_{IV}$ , respectively.

The application of rhenium as an alloying element results in the precipitation of topologically close-packed (TCP) phases well known for the system under study, such as  $\sigma$ ,  $\chi$ , and P phases. Such TCP phases are characterized by a high content of alloying high-melting-point elements in an alloy, and their precipitation results in the loss of solid solution strengthening of the  $\gamma$  matrix. In an alloy structure, TCP phases can exist in the form of smooth planes, which often serve as the sites of crack nucleation. The precipitation of TCP phases in the form of fine coherent particles promotes alloy strengthening [6, 7]. Based on the well-known data and our results, we present the following information on the TCP phases in the VKNA-25 alloy under study.

$\sigma$ -Phase particles (space group  $P4_2/mnm$ ) have acicular (transversal sizes about 0.1  $\mu\text{m}$ , length 0.5–25  $\mu\text{m}$ ) and platelike (width up to 3  $\mu\text{m}$ , length up to 7  $\mu\text{m}$ ) shapes. On the basis of the elemental composition of the particles determined by X-ray spectral microanalysis, we write the compound formula as  $(\text{Ni}, \text{Co}, \text{Re})(\text{Cr}, \text{Mo}, \text{W})$ . It should be noted that globular precipitations with a similar chemical composition are observed in the images of polished sections in the region of location of acicular and plate-like particles (Fig. 1b, region of a fine mixture  $\gamma + \gamma'_{II}$ ). These particles are assumed to be  $\sigma$ -phase particles in their cross section.

$\chi$ -Phase precipitates (space group  $I\bar{4}3m$ , structure type  $\text{Fe}_{18}\text{Cr}_6\text{Mo}_5$ ) are observed in the course of long-

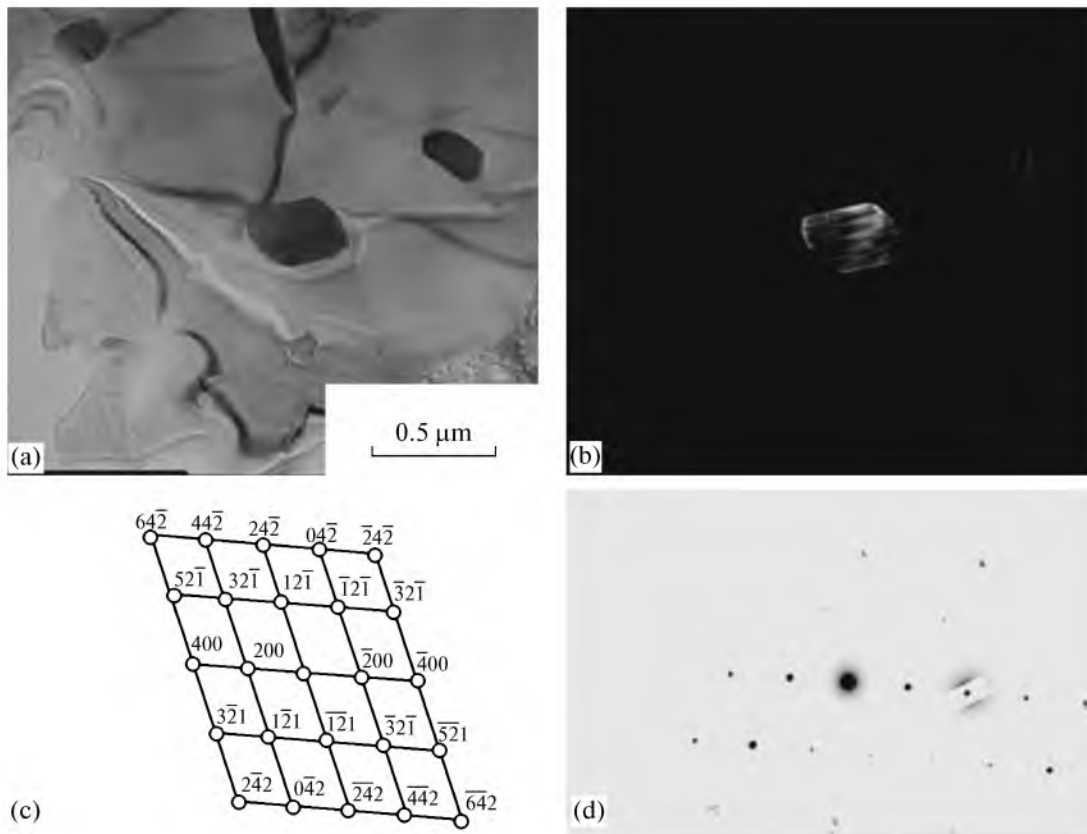


**Fig. 2.** Electron-microscopic image of a  $\chi$ -phase particle in the VKNA-25 alloy (annealing at 1100°C, 563 h): (a) bright-field image, (b) dark-field image taken with the  $[\bar{2}00]_{\chi}$  reflection, (c) key pattern, and (d) electron diffraction pattern.

term annealing in  $\gamma + \gamma'_{II}$  regions in the form of faceted 0.5- $\mu\text{m}$  particles (Fig. 2).

*P-Phase precipitates* (space group  $Pbnm$ , structure type  $\text{Cr}_9\text{Mo}_2\text{Ni}_{20}$ ) are coherent to the  $\chi$  phase and are observed in  $\gamma + \gamma'_{II}$  regions in the form of faceted particles (Fig. 3).

As follows from the alloy microstructure after annealing at 1100°C for 563 h, the precipitated  $\gamma'_{IV}$ -phase particles have an average size of  $20 \pm 3$  nm (Fig. 1a). Decomposition  $\gamma'_I \rightarrow \gamma + \gamma'_{III}$  is not observed.

As a result of alloying with lanthanum and long-term annealing, 3- $\mu\text{m}$  particles precipitate in the alloy structure. The content ratio of nickel to lanthanum in these particles corresponds to  $\text{Ni}_3\text{La}$  (Fig. 4).

As demonstrated by the studies of the VKNA-25 alloy containing 0.3 % La, particles with a high rhenium content (up to 10 at %) form in the material volume upon creep at 1100°C for 563 h. According to [1], VKNA-type alloys with rhenium are characterized by the precipitation of  $\text{Al}_{12}\text{Re}$  and  $\text{Al}_6\text{Re}$  particles. Since

rhenium belongs to elements increasing the solidus temperature of  $\text{Ni}_3\text{Al}$ -based alloys [8] and, hence, decreasing the diffusion mobility of atoms in an alloy, the precipitation of these particles results in a decrease in the rhenium content in the main  $\gamma$  and  $\gamma'$  phases. This is accompanied by significant microstructure variations. Microstructure images demonstrate dynamic recrystallization in local regions in this state (Fig. 5). Moreover, the morphology of the  $\gamma$  phase also changes as a result of high-temperature creep. The  $\gamma$  phase in the state after long-term annealing exists in the alloy in the form of quasi-continuous network in fine mixture  $\gamma + \gamma'_{II}$  regions; after long-term creep,  $\gamma$ -phase precipitations form small islands mainly extended along the direction perpendicular to the deformation direction. In such cases, topological inversion takes place in a microstructure.

Fracture during creep tests (1100°C,  $\sigma = 95$  MPa, time to failure 563 h) occurs as a result of pore formation at the boundaries of large  $\gamma'_I$ -phase precipitates and a fine  $\gamma + \gamma'_{II}$  mixture and at the interfaces particle-TCP phase matrix and lanthanum-containing

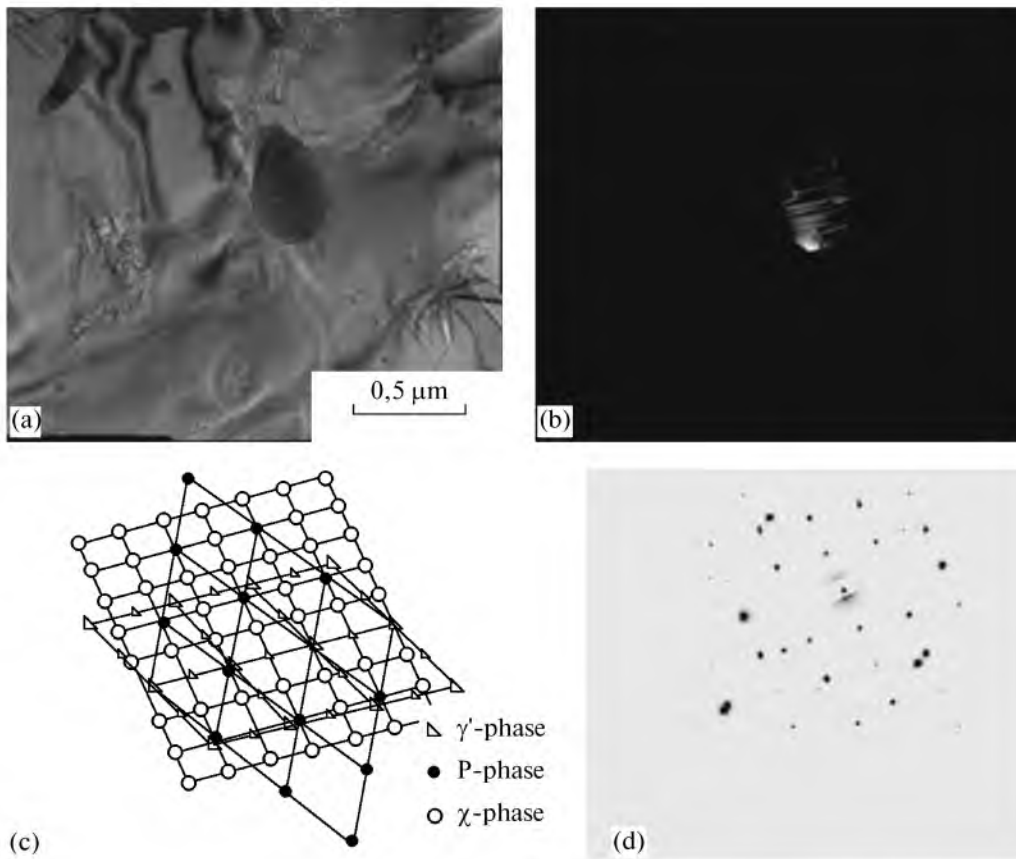


**Fig. 3.** Electron-microscopic image of a P-phase particle in the VKNA-25 alloy (annealing at 1100°C, 563 h): (a) bright-field image, (b) dark-field image taken with the  $[200]\chi$  reflection, (c) key pattern, and (d) electron diffraction pattern.

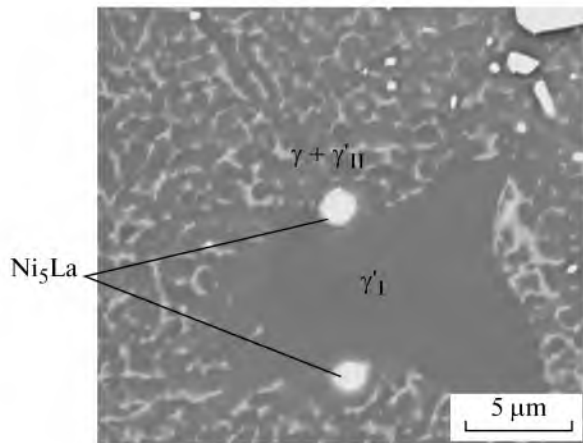


**Fig. 4.** Microstructure (SEM) of the VKNA-25 alloy after annealing at 1100°C, 563 h.

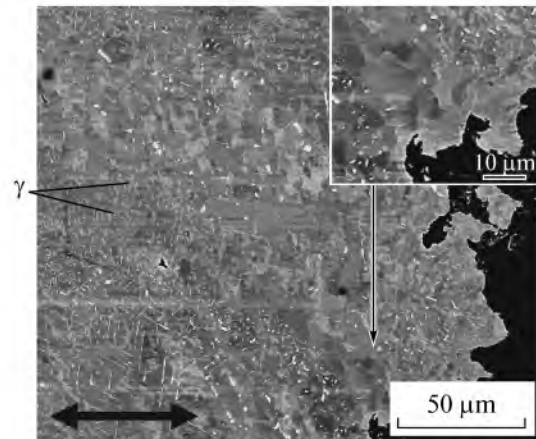


**Fig. 5.** Microstructure of the VKNA-25 alloy after high-temperature creep (longitudinal cross section). The black arrow indicates the deformation direction.

phases. Pore formation is likely to be related to the Kirkendall effect, which is caused by diffusion transfer of elements with significantly different partial diffusion coefficients during creep [1, 9].

## CONCLUSIONS

(1) Alloying of a VKNA-25 alloy with high-melting-point and rare-earth metals results in the precipitation of a large number of secondary phases repre-

sented by TCP phases ( $\sigma$ ,  $\chi$ , P) and lanthanum-based particles ( $\text{Ni}_5\text{La}$ ).

(2) The formation of  $\gamma'_{\text{IV}}$ -phase nanoparticles, which are secondary precipitates from a supersaturated nickel-based  $\gamma$  solid solution, is revealed in the structure of the VKNA-25 alloy.

(3) The fracture of the VKNA-25 alloy during high-temperature creep occurs due to pore formation, which is likely to be related to the Kirkendall effect.

#### REFERENCES

1. Yu. R. Kolobov, E. N. Kablov, E. V. Kozlov, et al., *Structure and Properties of Intermetallic Compounds with Nanophase Strengthening* (MISiS, Moscow, 2008) [in Russian].
2. Yu. R. Kolobov, *Diffusion Controlled Processes at Grain Boundaries and the Ductility of Metallic Polycrystals* (Nauka, Novosibirsk, 1998) [in Russian].
3. *New Materials: Collection of Articles*, Ed. by Yu. S. Karabasov, (MISiS, Moscow, 2002) [in Russian].
4. K. B. Povarova, A. A. Drozdov, N. K. Kazanskaya, A. E. Morozov, Yu. R. Kolobov, T. N. Verzhinina, and E. V. Kozlov, "Rare-Earth Metals (REMs) in Nickel Aluminide-Based Alloys: II. Effect of a REM on the Phase Composition of a Multicomponent  $\text{Ni}_3\text{Al}$ -Based Alloy," *Izv. Ross. Akad. Nauk, Ser. Met.*, No. 5, 48–56 (2008) [*Russian Metallurgy (Metally)*, No. 1, 398–405 (2008)].
5. E. V. Kozlov, B. L. Nikonenko, N. A. Koneva, and N. A. Popova, "Morphology of  $\gamma'$ -Phase in Alloys Based on  $\text{Ni}_3\text{Al}$ ," *Deformatsiya i Razrushenie Materialov*, No. 3, 44–47 (2006).
6. E. N. Kablov, *Cast Blades of Gas Turbine Engines* (MISiS, Moscow 2001) [in Russian].
7. Ch. T. Sims, *Superalloys II. Vol. 1. High-Temperature Materials for Aerospace and Industrial Power* (Metallurgiya, Moscow, 1995) [in Russian].
8. E. N. Kablov, "Physicochemical and Technological Features of Development of High-Temperature Alloys Containing Rhenium," *Vestn. Mosk. Univ., Ser. 2, Khim.* **46** (3), 155–167 (2005).
9. J. Duszczyk, J. Zhou, L. Marvina, and L. Z. Zhuang, "The Characteristics of the Diffusion between the As-Reaction-Formed  $\text{Ni}_3\text{Al}$  Intermetallic Compound and Pure Nickel for Interfacial Bonding," *J. Mater. Sci. Lett.*, No. 18, 111–113 (1999).